

# Detailed Evaluation of CFD Predictions against LDA measurements for flow on an aerofoil

A. Benyahia<sup>1</sup>, E. Berton<sup>1</sup>, D. Favier<sup>1</sup>, C. Maresca<sup>1</sup>, K. J. Badcock<sup>2</sup>, G.N.Barakos<sup>2</sup>  
1 LABM, 163, Avenue de Luminy, Case Postale 918 13288 MARSEILLE Cedex 09, FRANCE,  
benyahia@morille.univ-mrs.fr  
2 University of Glasgow, Glasgow G12 8QQ, U.K, gnaa36@aero.gla.ac.uk

**Keywords:** boundary layer, Embedded LDA, RANS

## Abstract:

The current work is the validation of the Glasgow flow solver PMB for static and moving aerofoils against data measured at LABM. The treatment of turbulence and transition is considered. Measurements made at LABM using an Embedded Laser Doppler Velocimetry (ELDVS technique) provide detailed boundary layer measurements on a pitching NACA0012 aerofoil. Flow laser sheet visualisation was used to characterize the transition behaviour. Finally, balance measurements of the lift and drag were made. After the measurements had been collected some RANS calculations were carried out. The detailed comparisons with the measured boundary layer profiles highlighted some difficulties, particularly with regard to the influence of the methods used for applying transition. Once fixed the agreement was much improved.

## 1 Introduction

The prediction of boundary layer behaviour on moving aerofoil sections is a necessary step towards the representation of dynamic stall which is experienced on the retreating blade of a helicopter rotor in forward flight. Blades in motion can benefit from a delay in the static angle of stall due to the re-energising influence of the motion on the boundary layer. However, the eventual stall is abrupt. Prediction of dynamic stall is difficult because it requires the resolution of smooth body separation which in turn is influenced by turbulence. In addition, since the crucial separation is close to the leading edge, transition plays an important role, even at high Reynolds' number. The prediction of dynamic stall using CFD is a key unsolved problem of rotor aerodynamics. RANS predictions give the time averaged boundary layer behaviour. However, the validation of RANS codes is usually done using pressure or force data, since this is what is most commonly available. More recently, with advances in laser based measurement techniques, velocity measurements are becoming available. This creates opportunities for a more direct validation of the RANS predictions relevant to dynamic stall, namely the boundary layer behaviour. The current report documents the validation of the Glasgow flow solver pmb for static and moving aerofoils against boundary layer data measured at LABM. The treatment of turbulence and transition is considered.

## 2 Experimental Setup

### 2.1 Test Cases

The cases considered here are for a NACA0012 aerofoil with a root chord of 0.3m. The wing used in the experiments spans the tunnel which has a test section of 1m by 0.5m and a length of 3m. The freestream velocity can be varied between 5 and 25 m/s and the natural turbulence intensity is less than 0.5%. The velocity used for the cases in this paper was 5 m/s. Since the RANS solver is formulated for compressible flows the computations have all been done for a freestream Mach number of 0.2, which is not expected to introduce compressible effects and so influence the solution behaviour. Three cases are considered. The first two are for flow around the fixed section, first at six degrees incidence and the secondly at fifteen degrees. Finally, a forced motion case is considered, with a sinusoidal motion applied about the quarter chord at a frequency of 1 Hz, which gives a reduced frequency (based on the chord and freestream velocity) of 0.188.

## 2.2 Data Acquired

The Embedded Laser Doppler Velocimeter (ELDVI) has an optical head mounted on a supporting turntable linked to the oscillating frame as sketched in figures 1 and 2. The optical head is equipped with a beam-expander in order to increase the focal distance up to 400 mm. The laser beams focus through a 45 deg mirror at a given position in chord and span. The supporting turntable is linked with the oscillating frame, so that U and V velocity components can be directly measured in the same reference frame of the motion. Due to the periodicity of the motion, each period is considered as a specific sample of the same phenomenon. So, each velocity component is recorded at each phase angle  $\omega t$  between 0 deg and 360 deg by steps of 0.703 deg over a large number of periods. Data are then statistically analyzed at prescribed values of the period, e.g. the instantaneous incidence, with an uncertainty of:

$$\delta\alpha=4\Delta\alpha/360=24/360=0.066\text{deg} \quad (1)$$

Data acquisitions are made on a microcomputer from two Burst Spectrum Analyzer (BSA) delivering the values of the two components U and V together with the arrival validation time for each frequency measurement. The software used for acquisition and data reduction (COMBSA) was developed at LABM under the Apple LABVIEW system.

The unsteady data reduction is performed using an ensemble average procedure suited for periodic flows investigation as described below. During a boundary-layer survey (s/C fixed) and for each normal distance y above the wall, 38 blocks of 512 values are acquired which correspond to 19456 measurements of U and  $t_u$  (arrival validation time of U) and the same number for V and  $t_v$ . The two BSA work in a master-master mode : the (U,V) acquisition is independently performed with the same time origin. Moreover, this particular acquisition mode is coupled with a «dead time» function which makes sure that only one particle can be validated during a fixed time interval (here  $\Delta t = 10^{-4}$ s). This function avoids the simultaneous validation of a burst of particles. Based on such options, the oscillation cycle number varies in a range between 150 and 300 depending on the flow configuration (with or without separation). Finally, one data file containing the 19456 data lines ( $t_u$ , U,  $t_v$ , V) is created for each normal distance y and the analysis software, provides the phase averaged ( $\langle U \rangle$ ,  $\langle V \rangle$ ) velocity components and their associated RMS quantities<sup>1</sup>. Indeed, due to the periodicity of the flow, each period is considered as a specific sample of the same phenomenon, so that each velocity component can be obtained at each phase angle  $\omega t$  as the averaged value of the velocity samples recorded at the same given phase angle and over a large number of oscillation cycles (greater than 150).

The negative arrival times due to the internal clock reset of the BSA are cut out in the first step. In the second step, the oscillation cycles are counted to keep only the common  $N_c$  cycles corresponding to the U and V simultaneous measurements. In the third step, the  $N_c$  cycles are pooled to obtain only one fictitious cycle. This cycle is split up into different divisions (512 in the present study) where velocities are averaged in order to provide discrete equidistributed representations of U and V velocities, written as  $\langle U \rangle$  and  $\langle V \rangle$ . The discrete representation obtained (512 points) results for each division, from an average of measurements from one or different cycles. Indeed, the division length (which represents  $2.10^{-3}$  second for a typical frequency of 1Hz), appears to be larger than the «dead time» interval fixed to  $\Delta t = 10^{-4}$ s.

The next step is to produce a Fourier series (256 harmonics) representing the two mean functions of velocity components (written as  $\tilde{U}$  and  $\tilde{V}$ ) in pitching motion case. The fluctuating quantities  $u'$  and  $v'$  can be then calculated by :

$$u'_n(t) = U_n(t) - \tilde{U}(\omega t), \quad v'_n(t) = V_n(t) - \tilde{V}(\omega t).$$

Then the RMS intensities are defined by:

$$\sigma_u(t) = \sqrt{\frac{1}{N_u} \sum_{n=1}^{N_u} [u_n(t)]^2} \quad (2a)$$

$$\sigma_v(t) = \sqrt{\frac{1}{N_v} \sum_{n=1}^{N_v} [v_n(t)]^2} \quad (2b)$$

Where  $N_u$  and  $N_v$  are respectively the number of U and V velocity component values included in one division.

All these fluctuating quantities are presented according to the phase averaged procedure, by representing the  $\langle U \rangle$ ,  $\langle V \rangle$ ,  $\langle u' \rangle$ ,  $\langle v' \rangle$ ,  $\langle \sigma_u(t) \rangle$ ,  $\langle \sigma_v(t) \rangle$  and  $\langle u' v' \rangle$  quantities as a function of the normal distance y to the surface.

Finally, A particular attention has been paid to the process used for the turbulence determination from the velocity signal. Thus, the new procedure of data acquisition involves only a given phase that can be repeated along the oscillation cycle. This acquisition procedure "phase by phase" makes sure that velocity components are measured by the ELDV method, along the same cycle and at the same time. This condition secures the validity of the velocity fluctuation measurements required for the Reynolds stress consideration.

### **3 Numerical Setup**

#### **3.1 Method**

Ken to add details of numerical method.

#### **3.2 Grids**

A structured grid was generated using the commercial code ICEMHEXA. This has a C-topology and has 89 points normal and 309 points wrapped around the NACA0012 section. There are 33 points in the wake and the first normal mesh spacing adjacent to the aerofoil is  $5 \times 10^{-5}$ . A coarser grid for convergence studies was created with half the number of points in each direction (i.e. 45 points normal and 155 points around the section).

#### **3.3 Calculation Details**

All calculations were run on a PC with a 750 MHz processor. It was found important to drive the residual down for both the fixed and pitching cases to ensure that the turbulence had developed fully and an equilibrium had been achieved.

For the fixed steady state case at six degrees incidence the solution converged in about 1600 implicit steps at a CFL number of 50. This required 1200 seconds of CPU time. The comparison of the boundary layer profiles for the KW and SA models on the different grids at  $x/c=0.67$  for the case with an incidence of six degrees is shown in figure 4. The agreement between the two sets of results is close.

For the fixed unsteady case at fifteen degrees incidence a reduced real time step of 0.07 was used to give 20 time steps per shedding cycle. The pseudo residual was dropped two orders of magnitude, typically requiring about 25 pseudo steps at each real time step. The total time for the calculation on the fine grid to reach a periodic state (after about 7 shedding cycles) was 10500 CPU seconds. The results obtained when halving the time step are very similar.

Finally, for the forced pitching case, at six degrees mean incidence and six degrees amplitude, 19 real time steps per cycle were used. It was found necessary to drive the pseudo residual down 3-4 orders in this case to obtain converged results. This required 300 pseudo steps per real time step for the first cycle and a half, and then, by restarting the pseudo convergence from the corresponding time on the previous cycle, this was reduced to less than ten pseudo steps per real time step thereafter. The influence of too lax a criteria is shown in figure 5 which shows that the loops thin as the tolerance is relaxed. The complete calculation on the fine grid took 25000 CPU seconds.

### **4 Fixed Cases Below Stall**

The Spalart-Allmaras,  $k-\omega$  and baseline SST turbulence models were evaluated for the flow at a fixed incidence of six degrees. In addition, the influence of the location of transition and the level of freestream turbulent kinetic energy was assessed. The last two factors turned out to influence the behaviour of the predictions much more than the model used and these are discussed in this section using the baseline SST model.

#### **4.1 Lift Curve**

The comparison between the measured and computed lift curves is shown in figure 6. At lower incidence the predictions and measurements are close to linear theory and are in good agreement. The predicted stall is earlier than in the experiments. The level of freestream turbulence has an influence as the stall angle is approached.

#### **4.2 Six Degrees**

In the experiments transition was observed between 0.1 and 0.3 of the chord. The behaviour of the predictions has been assessed for varying transition locations and freestream levels of turbulence.

First, plots of the turbulent Reynolds' number are shown in figure 7. All of these plots use the same scale and so comparison can be made between the plots. The major difference is introduced when using fully turbulent flow with a higher level of freestream turbulence. Large generation of turbulence is observed around the aerofoil nose and is then convected over the upper surface of the aerofoil. This is a well known artefact of linear eddy viscosity models [2]. Looking to the comparison of the boundary layer profiles at  $x/c=0.67$  as shown in figure 8, the influence of this behaviour, which is to thicken the boundary layer and make the profile more turbulent, is clear.

Applying transition away from the leading edge (in the middle of the observed transition region at  $x/c=0.2$ ), removes the problem of spurious generation of turbulence at the leading edge and improves the comparison with the measured profile for the larger value of freestream turbulence. Reducing the level of freestream turbulence for the fully turbulent flow has a similar effect on the profile obtained. For dynamic stall cases the state of the boundary layer at the leading edge is important and this behaviour of the turbulence model around the stagnation point may be very significant.

## 5 Fixed Case Above Stall

The case at 15 degrees incidence is observed in experiment to feature trailing edge shedding at a frequency of the order of 10 Hz, and hence a RANS solution should be unsteady. In experiment transition was observed to be very close to the leading edge at this incidence. For this more demanding case the turbulence model was found to have a significant influence of the flow topology predicted. Variants of the  $k-\omega$  model were used throughout this section. A low level of freestream turbulence has been applied to avoid excessive generation of turbulence at the leading edge.

Using the standard  $k-\omega$  model the solution is steady, with no shedding at the trailing edge. Relatively high levels of turbulence are predicted in the centre of the separated region, which arise from the turbulence model source terms reacting to velocity gradients which are not attributable to shear.

This is a common problem for Boussinesq based turbulence models and has been observed, for example, for delta wing flows [3]. A fix is to either reduce the production of turbulent kinetic energy or to enhance the production of the turbulent dissipation term according to the ratio of the magnitudes of the vorticity and strain rate tensors. When the vorticity is high, as in the region of separation, the scaling acts to reduce the turbulence, and when the strain rate is high, as in a boundary or shear layer, then the original model is recovered. The influence of this scaling is shown in figure 9 and indicates that the turbulence levels are reduced as expected. This flow field now allows vortex shedding to start at the trailing edge through separation of the recirculating flow to form a secondary separation. This was suppressed when the high levels of turbulence were present for the unscaled model.

An unsteady calculation was run using the scaled model for fully turbulent flow. The evolution of the lift coefficient to a periodic state is shown in figure 10. The reduced period is 1.6, indicated a reduced frequency of 0.51. A sequence of frames, shown in figure 11 shows a vortex being shed from the trailing edge. Time averaged boundary layer measurements at  $x/c=0.3$  and 0.67 are available for comparison. It was observed in the computations that the boundary layer profiles at these locations change very little in time and the profile from one instant is shown in figure 12. The comparison shows that the extent of the separated region is over-predicted when compared with experiment.

## 6 Pitching Aerofoil Case

Finally, a case in forced pitch is considered. The mean incidence and amplitude of the sinusoidal motion is six degrees and the frequency is 1Hz, leading to a reduced frequency of 0.188. Dynamic stall is not expected for this motion. From the static results the main influence of the transition is herefore expected to be from the production of turbulence around the stagnation point. For this case the baseline SST model has been used, with little difference being observed between these and the  $k-\omega$  results.

First, the lift loop is shown in figure 13, with reasonable agreement obtained. All cases generated negative values for the turbulent kinetic energy at some stage throughout the cycle and this was reset to freestream values to allow the calculation to continue. However, for very low values of freestream turbulence this ad-hoc treatment triggered massive separation and the results thereafter were unrealistic. These results are omitted. The influence of transition and freestream values of turbulence, with the exception of the case with high freestream turbulence and fully turbulent, on the solutions is seen to be limited. For this case it was seen for the static case that high levels of turbulence are created around the leading edge.

The comparison of boundary layer profiles, shown in figure 14, is very close throughout the pitching cycle.

## 7 Conclusions

## **Bibliography**

1. Berton, E. Favier, D., and Maresca., C, "Embedded L.V. Methodology for Boundary-Layer Measurements on Oscillating Models", *Proceedings of the Twenty-Eight Fluid Dynamics Conference*, AIAA, AIAA paper 97/1832, Snowmass, June 1997.
2. Barakos, G.N., "Study of Unsteady Aerodynamics Phenomena using advanced turbulence closures", PhD thesis, UMIST, 1999.
3. Brandsma, F.J., Kok, J.C., Dol, H.S. and Elsenaar, A., "Leading edge vortex flow computations and comparison with DNW-HST wind tunnel data". RTO/AVT Vortex Flow Symposium, Loen, Norway, 2001.

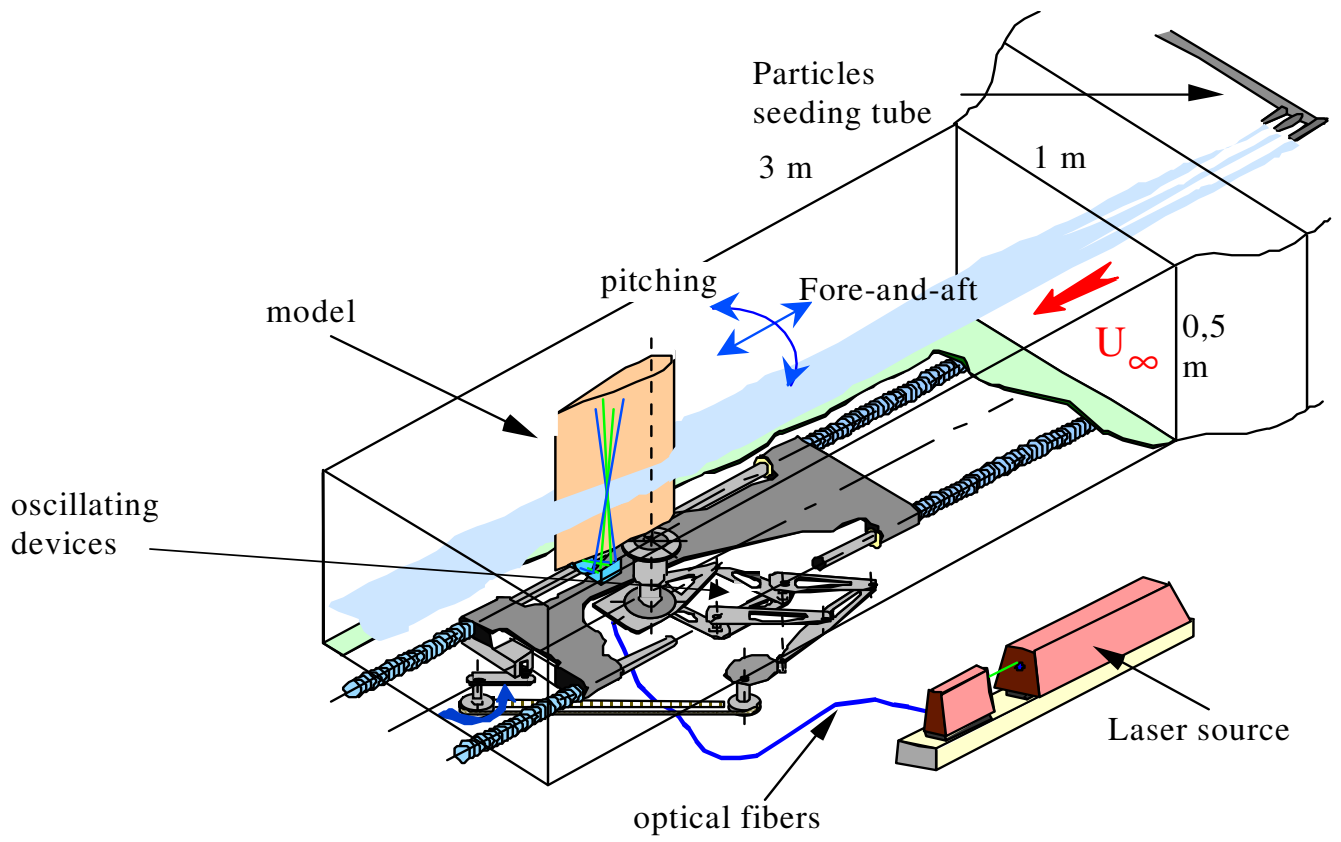


Figure 1: S2L low speed wind-tunnel, Experimental set-up

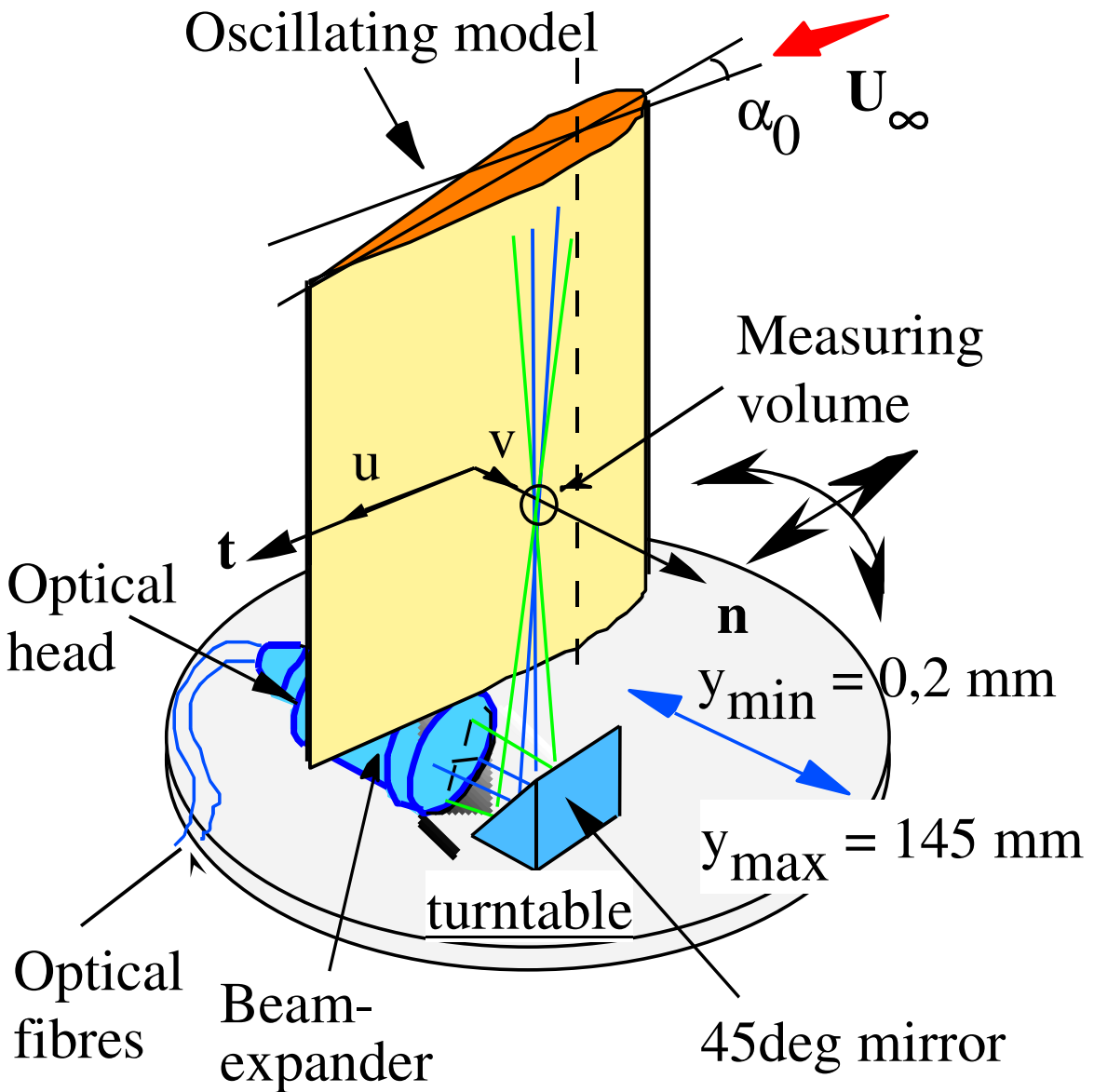


Figure 2: ELDV measurements linked with the oscillating frame model

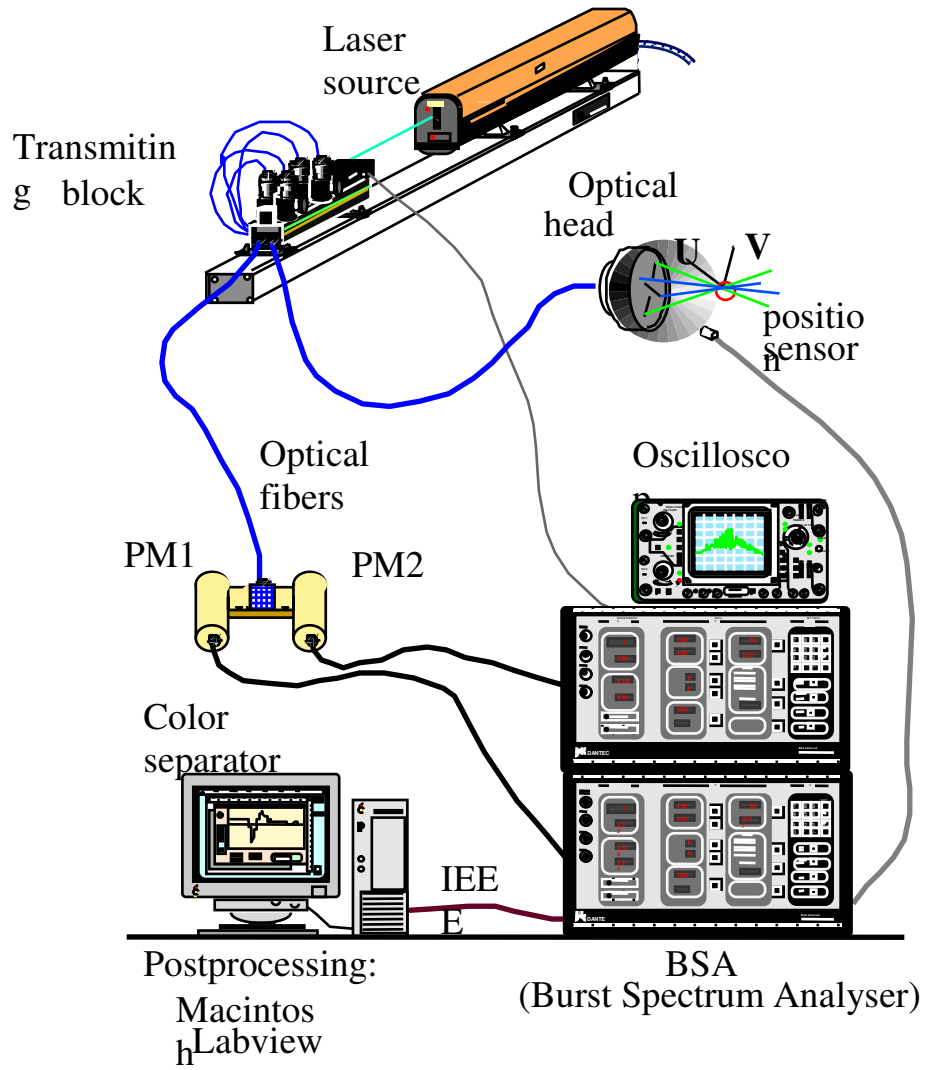


Figure 3: ELDV Acquisition chain

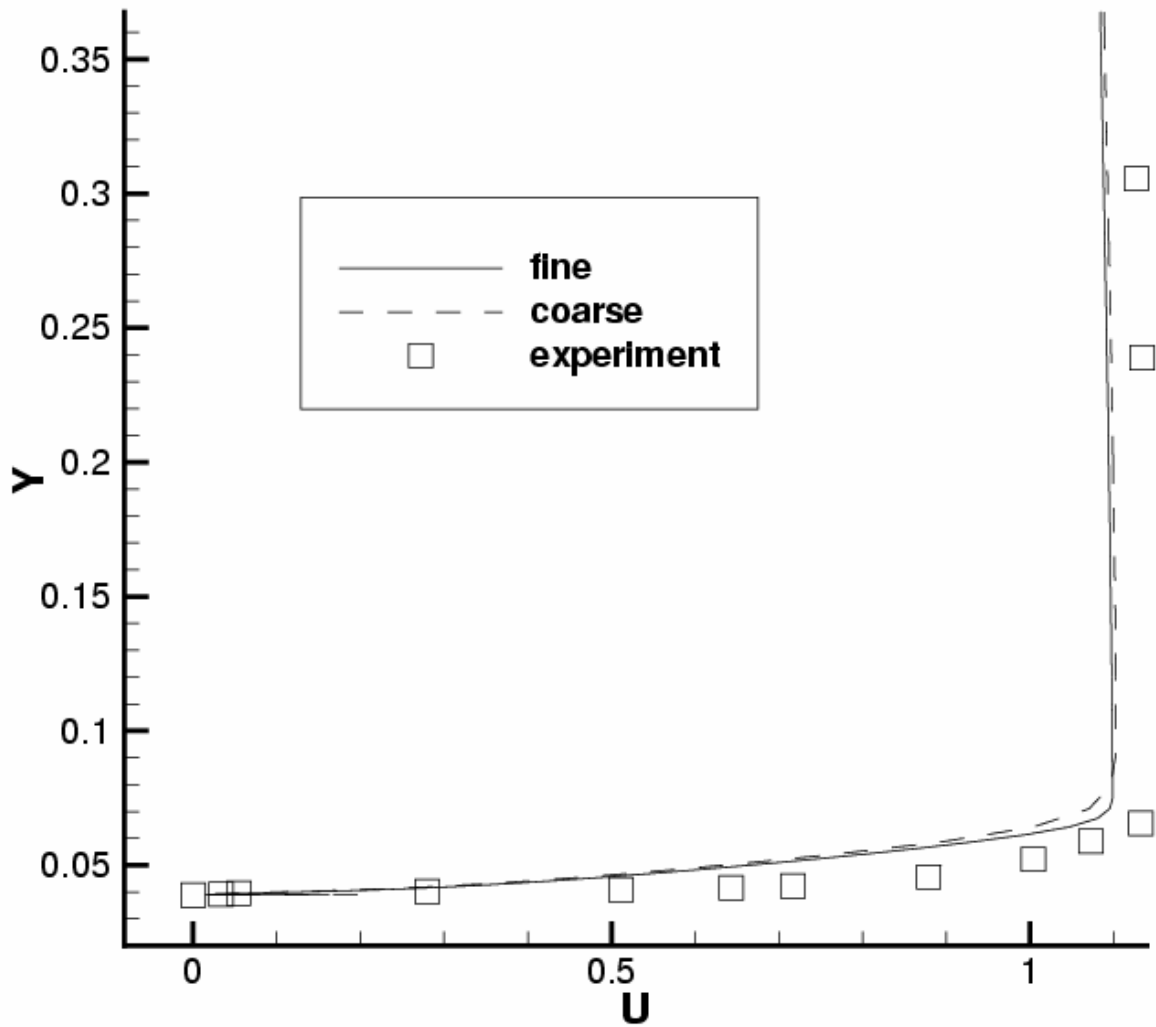


Figure 4: Comparison of predicted boundary layer profiles at  $x/c=0.67$  on the coarse and refined grids for the case with fully turbulent flow,  $k=0.001$  and a fixed incidence of six degrees.

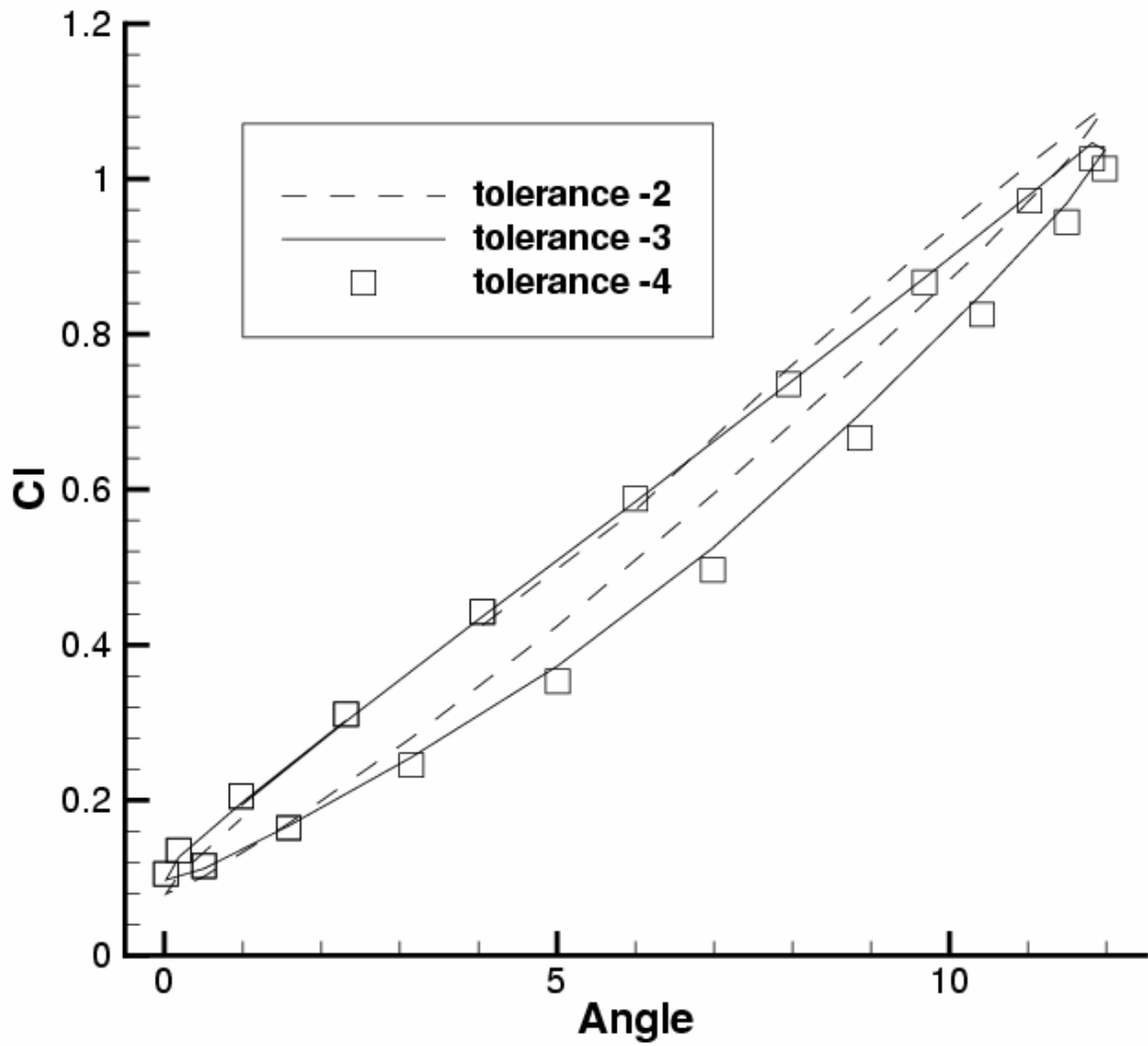


Figure 5: Influence of the pseudo time tolerance on the lift coefficient loop for the pitching case at six degrees mean incidence and an amplitude of six degrees.

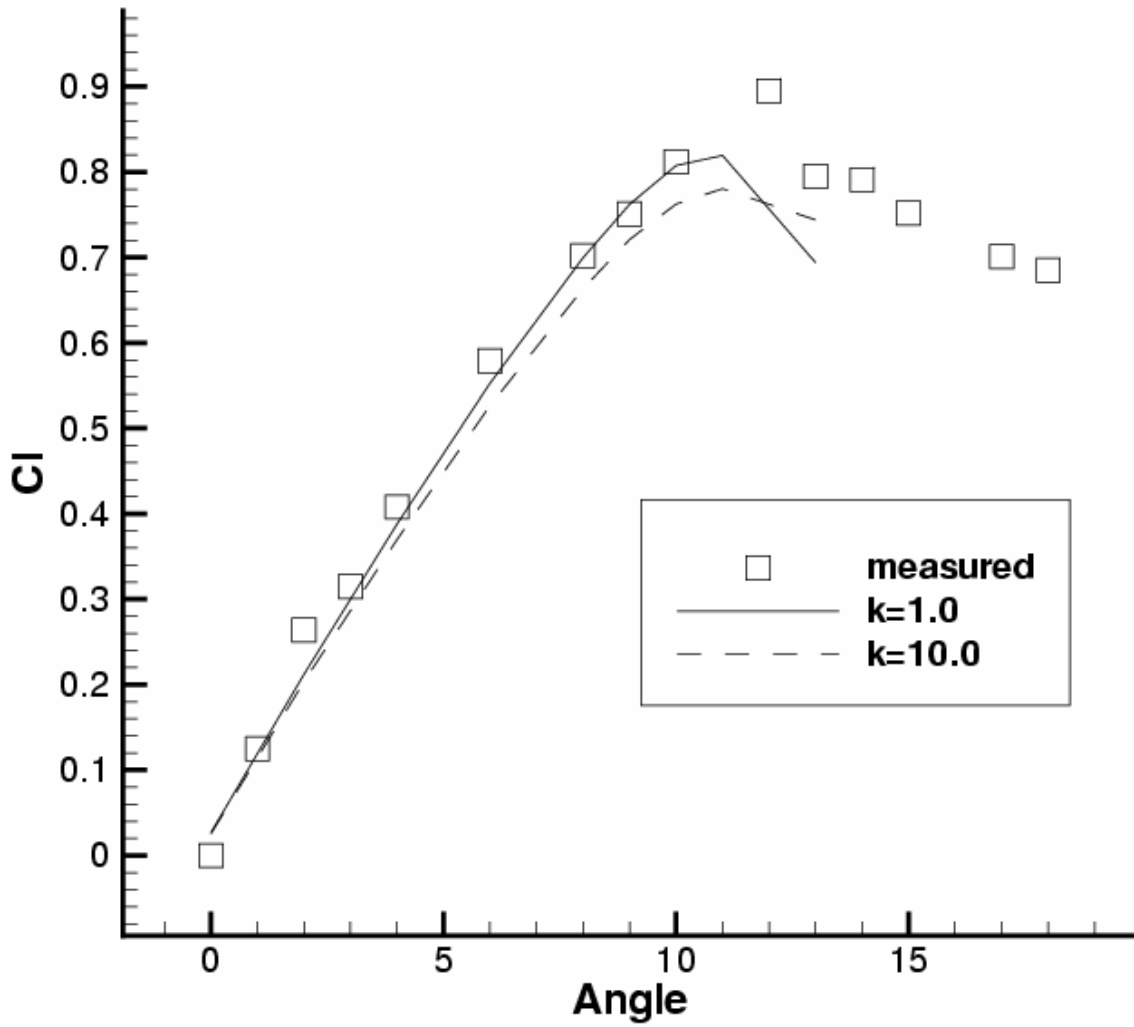
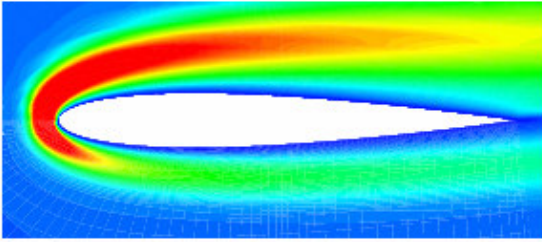
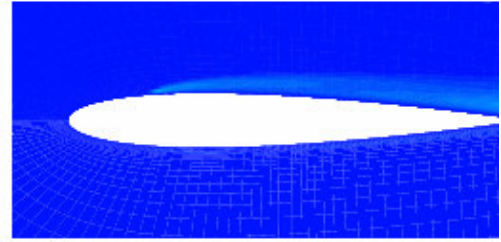


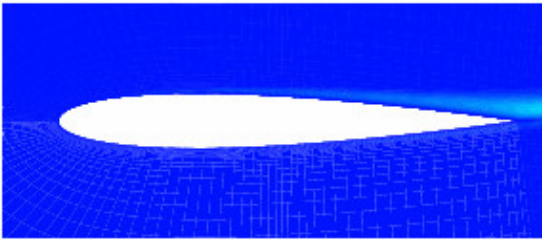
Figure 6: Comparison of lift curve with experiment for two levels of freestream turbulence.



fully turbulent and  $k=10$



transition at  $0.2$  and  $k=10$



fully turbulent and  $k=0.001$

Figure 7: Turbulent Reynolds' number for aerofoil at fixed incidence of six degrees for various locations of transition and freestream turbulence.

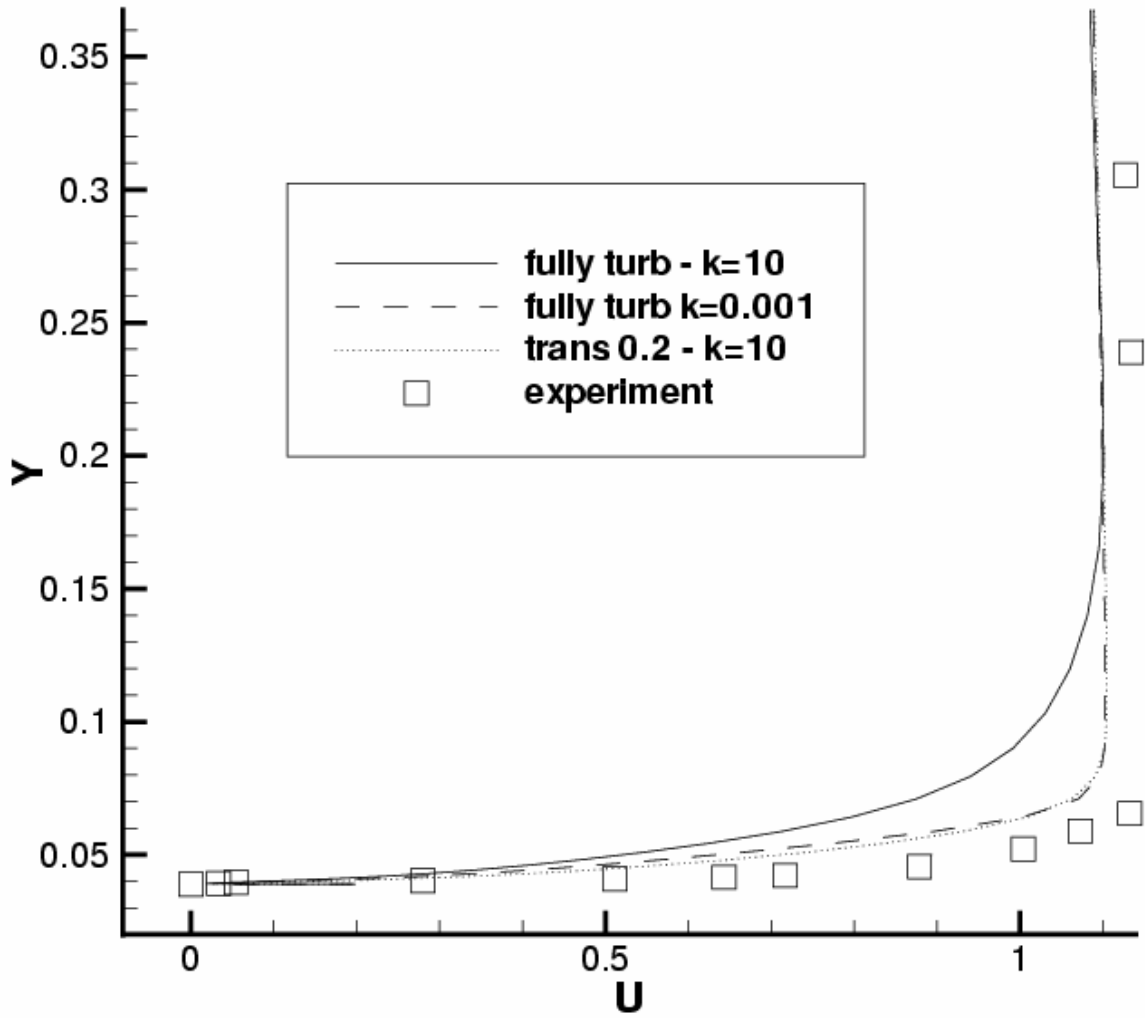


Figure 8: Comparison of boundary layer profiles for aerofoil at at fixed incidence of six degrees for various locations of transition and freestream turbulence.

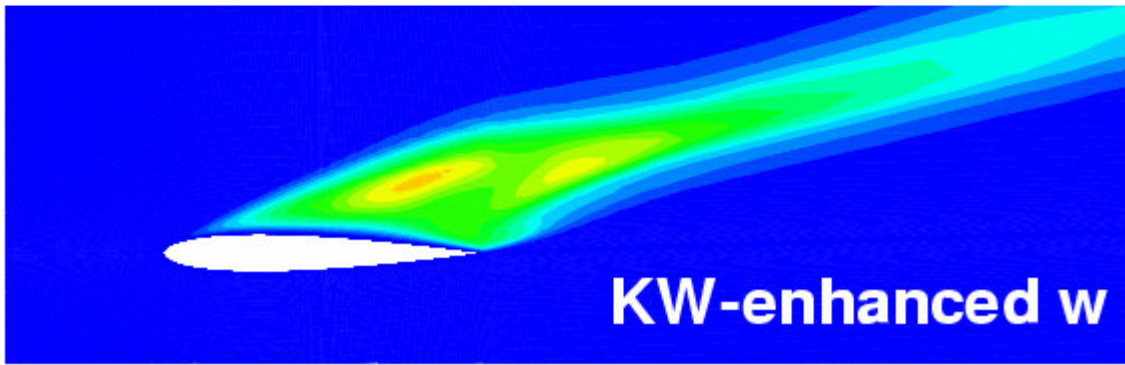
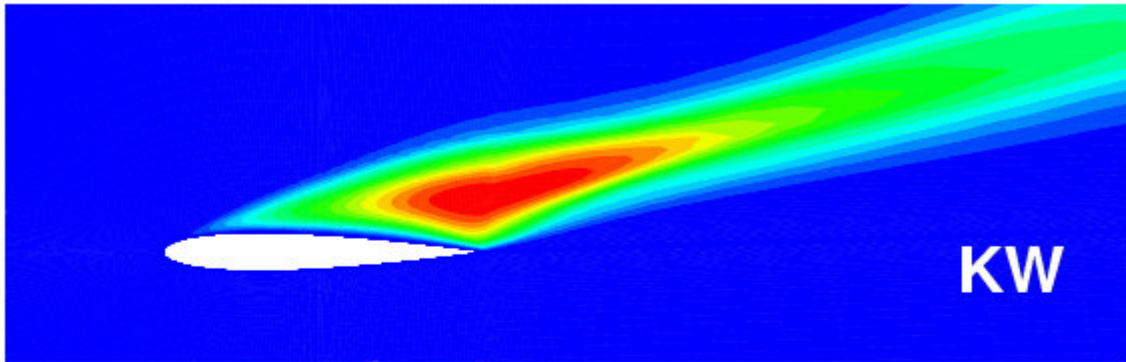


Figure 9: Turbulent Reynolds' number for aerofoil at fixed incidence of fifteen degrees using  $k-\omega$  model with enhanced destruction of turbulence and fully turbulent.

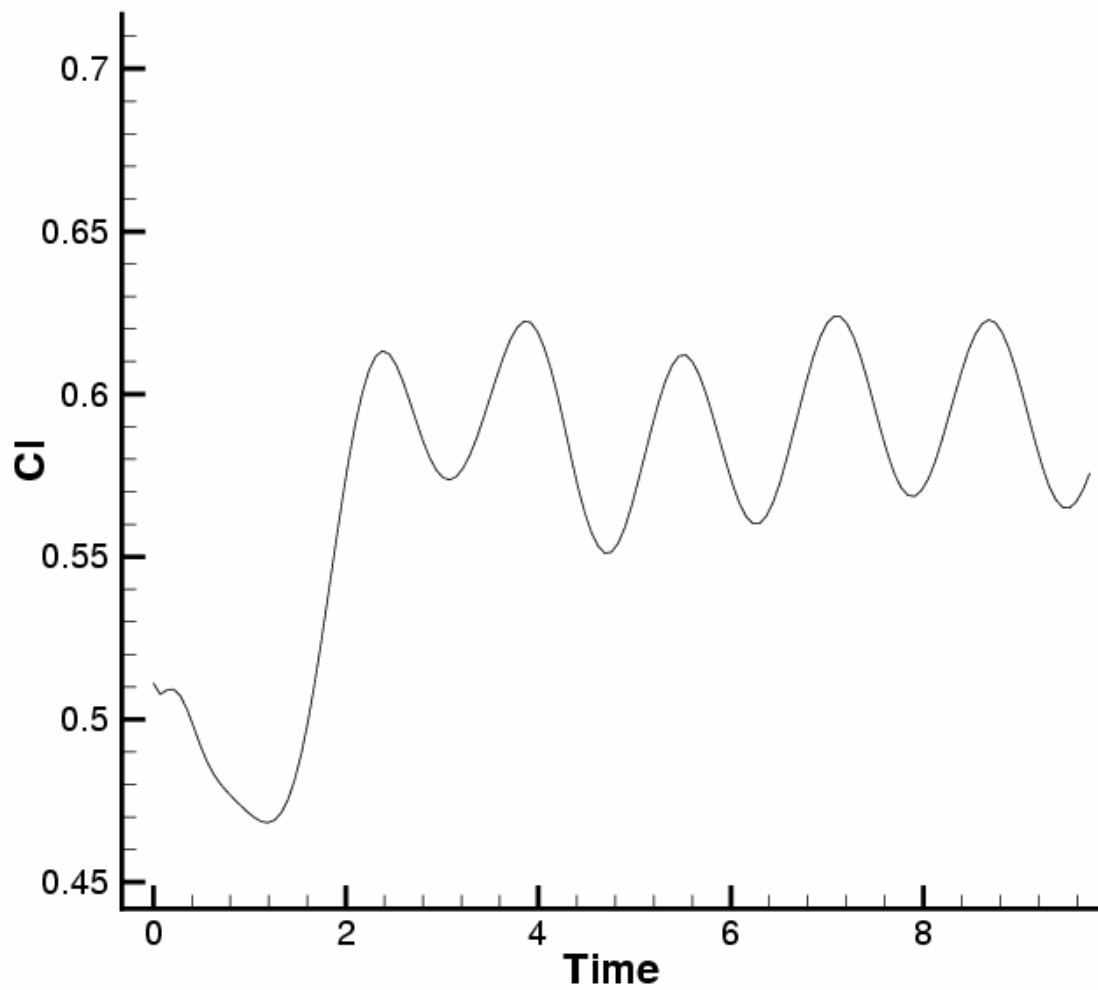


Figure 10: Time evolution of the lift coefficient for an aerofoil at a fixed incidence of fifteen degrees using  $k-\omega$  model with enhanced destruction of turbulence and fully turbulent.

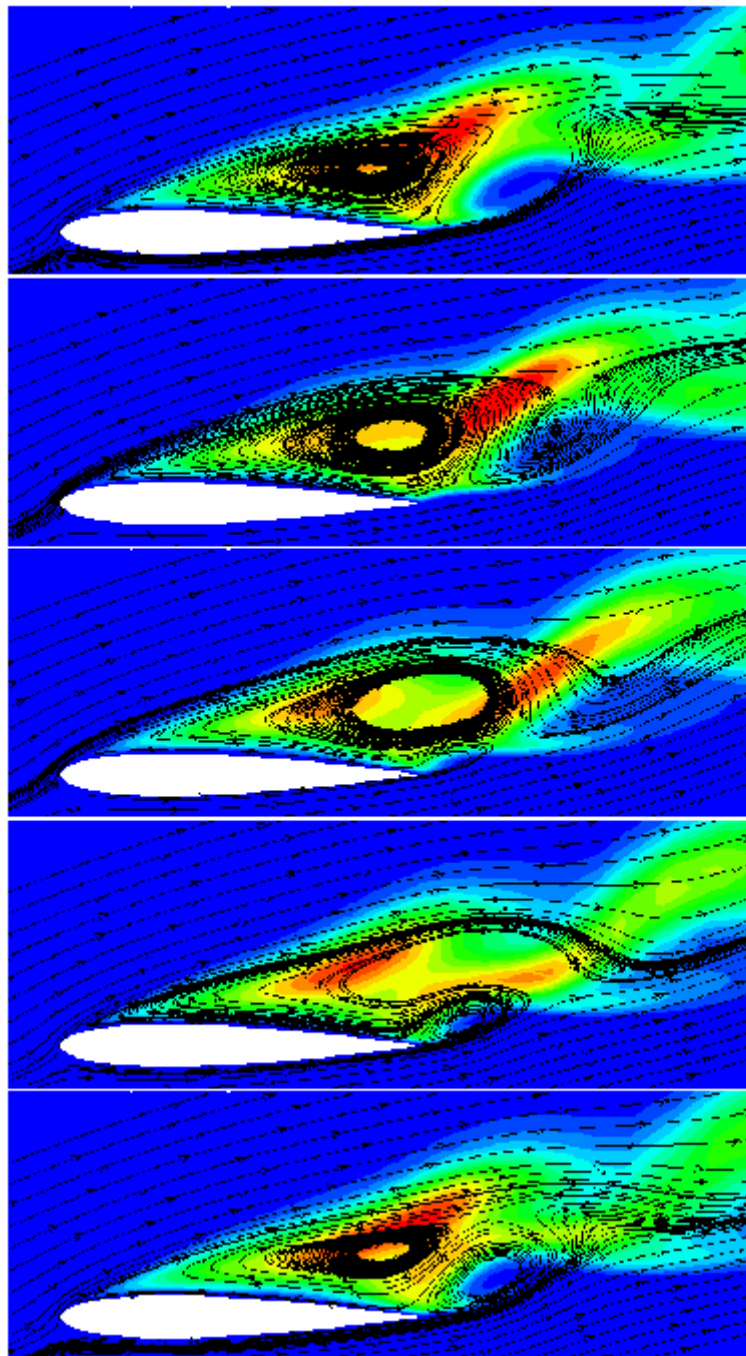


Figure 11: Vortex Shedding cycle for aerofoil at fixed incidence of fifteen degrees using  $k-\omega$  model with enhanced destruction of turbulence and fully turbulent.

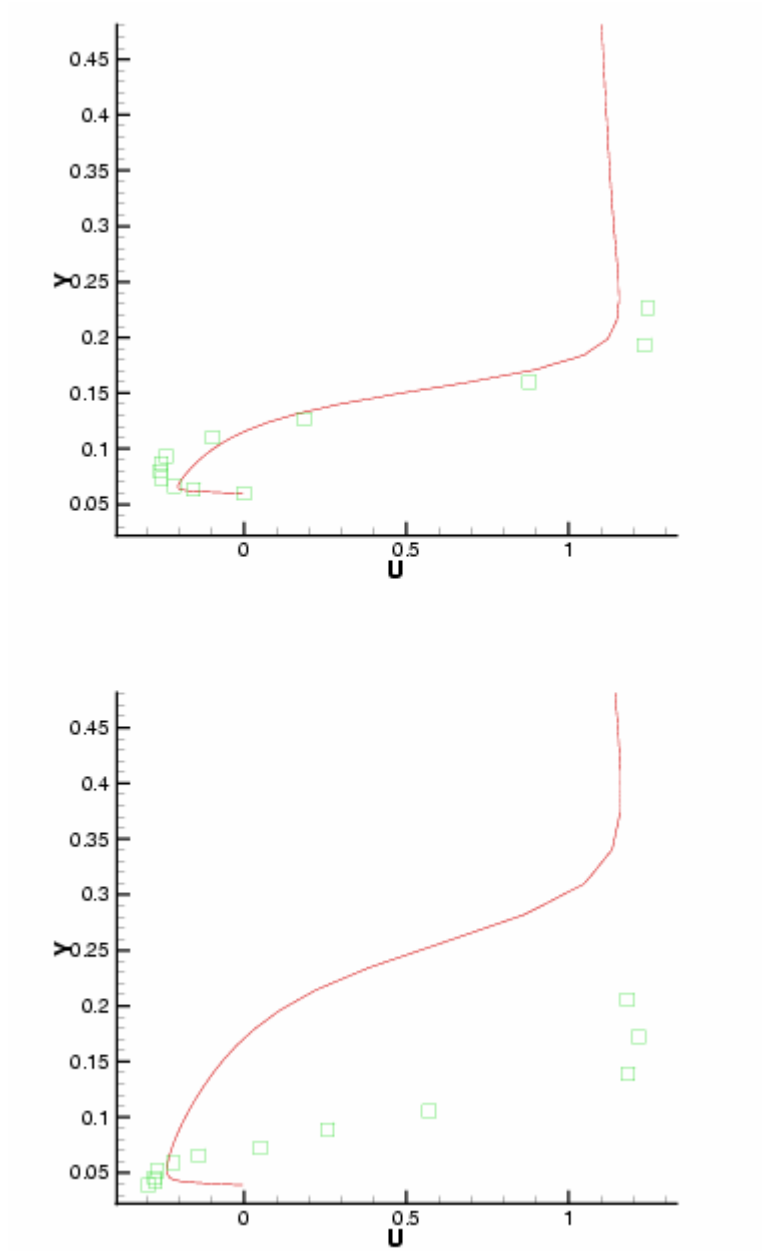


Figure 12: Comparison of Boundary Layer profiles for aerofoil fixed at fifteen degrees incidence using  $k-\omega$  model with enhanced destruction of turbulence and fully turbulent.

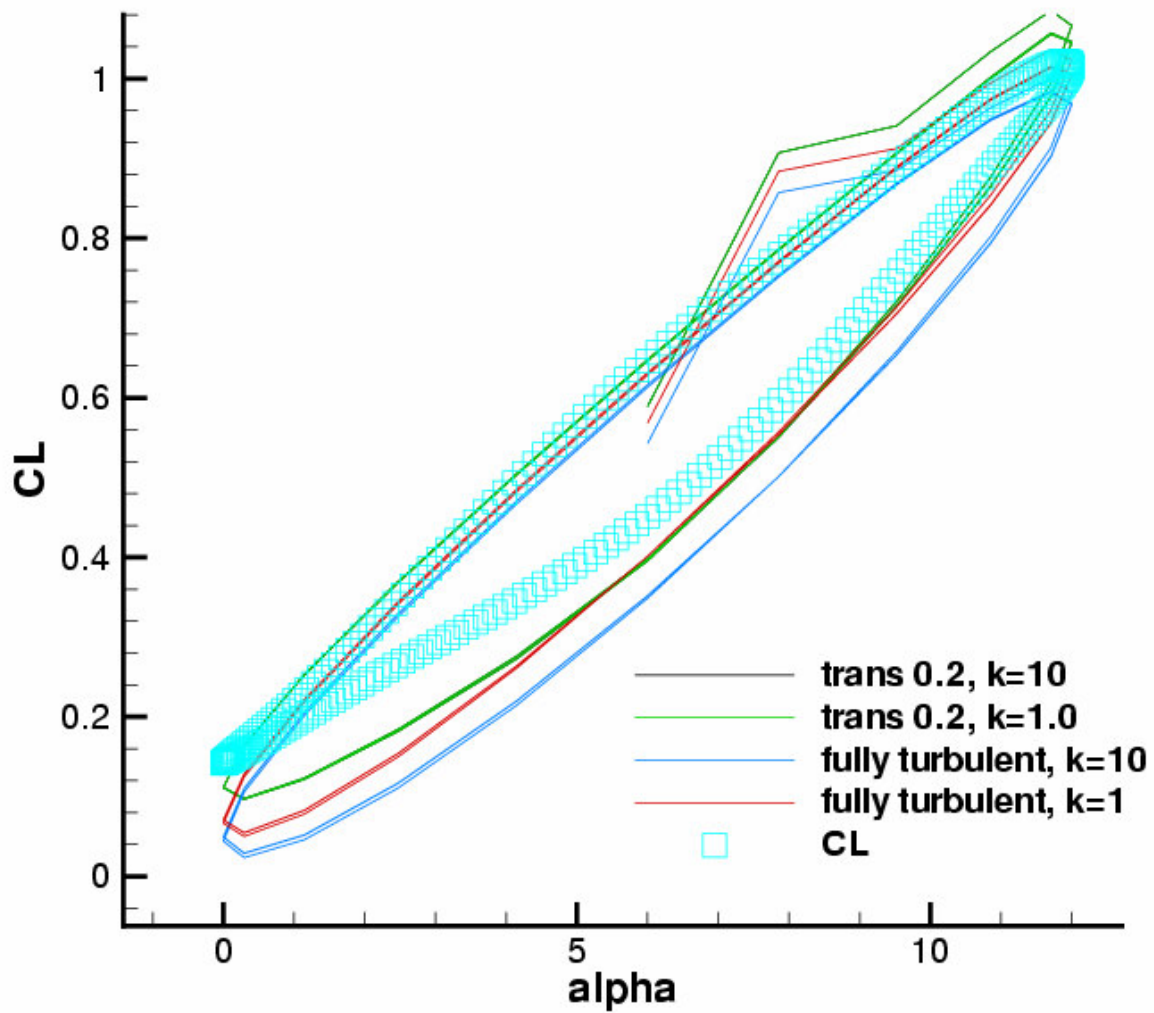


Figure 13: Comparison with experiment for the lift coefficient loop for the pitching case at six degrees mean incidence and an amplitude of six degrees.

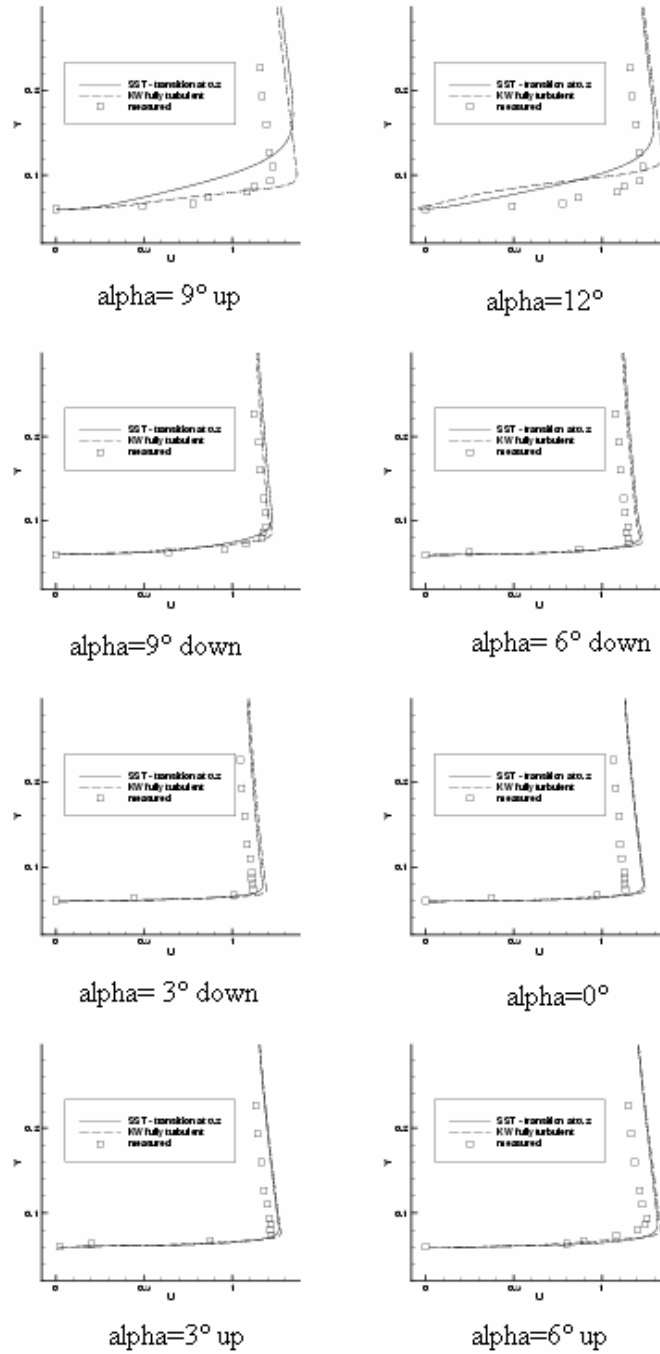


Figure 14: Comparison of boundary layer profiles for pitching aerofoil using SST model with fully turbulent flow.